HHS Public Access

Author manuscript

Pediatr Radiol. Author manuscript; available in PMC 2017 November 01.

Published in final edited form as:

Pediatr Radiol. 2016 November ; 46(12): 1651–1662. doi:10.1007/s00247-016-3672-1.

Feasibility, tolerability and safety of pediatric hyperpolarized ^{129}Xe magnetic resonance imaging in healthy volunteers and children with cystic fibrosis

Laura L. Walkup[1], **Robert P. Thomen**[1,2], **Teckla Akinyi**[1,3], **Erin Watters**[1], **Kai Ruppert**[1], **John P. Clancy**[4], **Jason C. Woods**[1,2], and **Zackary I. Cleveland**[1,3]

Zackary I. Cleveland: zackary.cleveland@cchmc.org

[1]Center for Pulmonary Imaging Research, Division of Pulmonary Medicine and Department of Radiology, Cincinnati Children's Hospital Medical Center, 3333 Burnet Ave., MLC 5033, Cincinnati, OH 45229, USA

[2]Department of Physics, Washington University in St. Louis, St. Louis, MO, USA

[3]Biomedical Engineering Program, University of Cincinnati, Cincinnati, OH, USA

[4]Division of Pulmonary Medicine, Cincinnati Children's Hospital Medical Center, Cincinnati, OH, USA

Abstract

Background—Hyperpolarized ^{129}Xe is a promising contrast agent for MRI of pediatric lung function but its safety and tolerability in children have not been rigorously assessed.

Objective—To assess the feasibility, safety and tolerability of hyperpolarized ^{129}Xe gas as an inhaled contrast agent for pediatric pulmonary MRI in healthy control subjects and in children with cystic fibrosis.

Materials and methods—Seventeen healthy control subjects (ages 6–15 years, 11 boys) and 11 children with cystic fibrosis (ages 8–16 years, 4 boys) underwent ^{129}Xe MRI, receiving up to three doses of ^{129}Xe gas prepared by either a commercially available or a homebuilt ^{129}Xe polarizer. Subject heart rate and SpO_2 were monitored for 2 minutes post inhalation and compared to resting baseline values. Adverse events were reported via follow-up phone call at days 1 and 30 (range ±7 days) post-MRI.

Results—All children tolerated multiple doses of ^{129}Xe, and no children withdrew from the study. Relative to baseline, most children who received a full dose of gas for imaging (10 of 12 controls and 8 of 11 children with cystic fibrosis) experienced a nadir in SpO_2 (mean −6.0 ± standard deviation 7.2%, $P \leq 0.001$); however within 2 minutes post inhalation SpO_2 values showed no significant difference to baseline ($P=0.11$). There was a slight elevation in heart rate (mean +6.6 ± 13.9 beats per minute [bpm], $P=0.021$), which returned to baseline within 2 minutes post inhalation ($P=0.35$). Brief side effects related to the anesthetic properties of xenon were mild and quickly resolved without intervention. No serious or severe adverse events were observed; in total,

Compliance with ethical standards

Conflicts of interest None

four minor adverse events (14.3%) were reported following ^{129}Xe MRI, but all were deemed unrelated to the study.

Conclusion—The feasibility, safety and tolerability of ^{129}Xe MRI has been assessed in a small group of children as young as 6 years. SpO_2 changes were consistent with the expected physiological effects of a short anoxic breath-hold, and other mild side effects were consistent with the known anesthetic properties of xenon and with previous safety assessments of ^{129}Xe MRI in adults. Hyperpolarized ^{129}Xe is a safe and well-tolerated inhaled contrast agent for pulmonary MR imaging in healthy children and in children with cystic fibrosis who have mild to moderate lung disease.

Keywords

Children; Cystic fibrosis; Hyperpolarized xenon; Lungs; Magnetic resonance imaging

Introduction

Driven by improved solid-state laser technology in the mid-1990s, it became possible to generate highly non-equilibrium total nuclear magnetic moment in the noble gas isotopes ^{3}He and ^{129}Xe. These hyperpolarized gases displayed approximately 10,000-fold enhanced MRI signal intensities, making it possible to generate MR images in seconds. As a result, hyperpolarized noble gases quickly emerged as promising inhaled contrast agents for pulmonary MRI [1–3], and since then the utility of hyperpolarized-gas MRI to visualize and quantify regional ventilation [4, 5] and assess alveolar airspace microstructural dimensions [6–9] has been demonstrated both in healthy volunteers and in subjects with a range of pulmonary diseases, including chronic obstructive pulmonary disease (COPD) [10, 11], cystic fibrosis (CF) [12, 13] and asthma [14–16]. It is important to note that unlike chest radiographs, scintigraphic ventilation/perfusion scanning and CT, hyperpolarized-gas MRI involves no ionizing radiation, and in stark contrast to lung biopsy (currently the gold standard for assessing alveolar structure), hyperpolarized-gas MRI is noninvasive, making the modality attractive for longitudinally assessing lung pathology. Reviews of hyperpolarized gas preparation [17, 18] and the translational applications in MRI are available elsewhere [19–22].

Hyperpolarized ^{3}He has historically been the preferred hyperpolarized-gas MRI contrast agent for pediatric pulmonary imaging [23–26], and indeed ^{3}He MRI has an established safety record for assessing pulmonary function in pediatric lung diseases, including CF [27–31] and asthma [32, 33], and quantifying normal alveolar growth during childhood and adolescence [34, 35]. Driven by the increasing scarcity and cost of ^{3}He [36] and substantial improvements in ^{129}Xe polarization technology, there has been a renewed interest in ^{129}Xe MRI [37–41]. A growing number of studies have demonstrated that hyperpolarized ^{129}Xe can provide regional measures of pulmonary ventilation (an assessment of lung function) and alveolar airspace microstructure (via ^{129}Xe diffusion imaging) comparable to those obtained from ^{3}He, providing a sustainable path for clinical translation of ^{129}Xe MRI [10, 42, 43]. Furthermore, xenon is moderately soluble in pulmonary tissues (Ostwald solubility ~10% [44]) and exhibits a large (>200 parts per million [ppm]) chemical shift range in the lungs, thus allowing hyperpolarized ^{129}Xe to serve as a regional probe of gas-exchange

dynamics [45–49]. However, its tissue solubility also makes the safety and tolerability of ^{129}Xe a greater concern than ^{3}He. Specifically, dissolved xenon can give rise to neurological effects that include anesthesia at sustained, elevated alveolar concentrations (alveolar concentration >63% [50]) and milder effects including euphoria and dizziness at lower alveolar concentrations [51].

Although reports demonstrate that hyperpolarized ^{129}Xe is a safe contrast agent for pulmonary imaging in adults [52, 53], the safety and feasibility of ^{129}Xe MRI in children has not been assessed. However there are reports of sub-anesthetic doses of xenon gas being safely administered to children undergoing xenon-enhanced CT [54, 55]. The most relevant work documenting the safety of xenon gas in children is that of Goo et al. [56], who performed Xe-enhanced CT in 17 pediatric patients (age range 7–18 years) with bronchiolitis obliterans. Subjects inhaled multiple breaths of 30% xenon to establish a steady-state exhaled Xe concentration of 25–30% (wash-in times ranged 36–90 s) before a breath-hold and CT acquisition (approximately 10 s), and the authors observed no significant changes in subject heart rate, SpO_2 or blood pressure. Transient, minor side effects related to the anesthetic properties of xenon, including peripheral numbness and dizziness, were reported in most subjects (70.6%); however these effects were deemed mild and resolved within a few minutes and without intervention [56].

This study assesses the safety of hyperpolarized ^{129}Xe MRI in a small group of children. For this initial assessment, we performed ^{129}Xe MRI in a cohort children with cystic fibrosis (n=11) and in healthy age-matched children (n=17) ranging 6–16 years old. In doing so, we investigated the safety and tolerability of xenon gas in children and also demonstrated the feasibility of ^{129}Xe MRI techniques in relatively young children with mild to moderate lung disease.

Materials and methods

Research subjects

Following U.S. Food and Drug Administration investigational new drug (IND 123,577) and institutional review board approvals, we enrolled 28 children (age range 6–16 years) in the study. Inclusion criteria included the ability to perform a 16-s breath-hold and, for the children with cystic fibrosis, a clinical diagnosis of CF based on standard guidelines [57]. Exclusion criteria included a history of poorly controlled asthma, history of heart defect, use of an asthma rescue inhaler ≥2 times in the last month, symptoms of respiratory or sinus infection 1 week prior to imaging, baseline pulse oximetry <95% at the time of MRI, pregnancy or positive pregnancy test, and standard MRI exclusions. We obtained written parental consent and age-appropriate subject assent for all subjects. Table 1 details demographics and clinical information for our subjects. We enrolled 17 healthy control subjects (11 boys, 6 girls, age range 6–16 years) and 11 children with diagnosed CF [58] (4 boys, 7 girls, age range 8–16 years). CF patient genotypes and CF-related pathogens are also provided in Table 1. In children for whom recent (within 6 months) clinical pulmonary function tests were not available, spirometry was performed immediately prior to MR imaging using a Koko portable handheld spirometer (nSpire Health, Longmont, CO) according to American Thoracic Society (ATS) guidelines [57].

Hyperpolarized ^{129}Xe gas preparation

Hyperpolarized ^{129}Xe gas was prepared using either a commercially available polarizer (Model 9800; Polarean, Durham, NC) or our center's homebuilt polarizer [59, 60]. ^{129}Xe was dispensed into a Tedlar delivery bag (600 ml or 1,000 ml, the latter if the dose was >600 ml; Jensen Inert Products, Coral Springs, FL) through 3/8″ tubing (Tygon; Saint-Gobain, Akron, OH). A mouthpiece (part number DK100191; Epsilon Medical Devices, Penang, Malaysia) or a custom mouthpiece designed by Teleflex (Morrisville, NC) was fitted to the tubing before delivery to the child. All experiments used isotopically enriched xenon gas (86% ^{129}Xe), and ^{129}Xe polarizations ranged 10–30% at the time of imaging. Xenon polarization was measured using a polarization measurement station (Model 2881; Polarean, Durham, NC) before gas administration.

MR imaging protocol

Children were imaged with a Philips 3-T Achieva MRI scanner using one of two homebuilt ^{129}Xe dual-looped saddle coils designed to fit either small or large subjects [61]. At the time of imaging, a visual assessment was made to determine which coil best matched a child's thoracic volume. After 3-plane ^{1}H localization scans, children received a bag of air with a volume approximately equal to one-sixth total lung capacity (TLC) to practice the inhalation and breath-hold maneuver (~16 s) during a conventional ^{1}H MRI gradient-echo scan. For each ^{129}Xe dose (calibration and imaging), the child was coached by a team member to exhale to functional residual capacity (FRC) before inhaling the ^{129}Xe gas mixture.

To set the scanner flip angle, α, a ^{129}Xe calibration dose consisting of ~250 ml of xenon and ~250 ml of N_2 (99.9999%, Praxair) was administered using the same breath-hold maneuver as described to determine the in vivo flip angle. Calibration was performed for each child individually by fitting the signal decay from 64 constant flip-angle whole-lung excitations (total duration ~2 s) to $S_n=S_0\cos^{n-1}(\alpha)$, where S_n is the signal magnitude of the n^{th} excitation.

Hyperpolarized ^{129}Xe ventilation images were acquired with linear phase encoding and a flip angle optimized for maximum signal at k-zero [62]. Additional imaging parameters included flip angle of 9–12°, repetition time/echo time [TR/TE] 8/4 ms, matrix size 52–96 × 96–144, voxel size 3 × 3 × 15 mm^3, 9–14 slices, with a total scan time of less than 16 s. For eight children, ^{129}Xe diffusion images were acquired using multiple b values (b = 6.25, 12.5, 18.75, 25 s/cm^2) bi-polar diffusion-sensitizing gradient-echo sequence [63] (flip angle 5–10°, diffusion time [Δ] 3.5 ms, lobe duration [δ] 3.1 ms, TR/TE 15/10 ms, matrix size 25–96 × 48–96, voxel size 3–7 × 3–7 × 15–30 mm^3, 4–10 slices), using a maximum scan duration of 16 s. ^{129}Xe apparent diffusion coefficient (ADC) maps were generated from the diffusion images using code written in MATLAB (MathWorks, Natick, MA) and the R language. Hyperpolarized ^{129}Xe chemical shift saturation recovery (CSSR) MR spectroscopy [48, 49] was performed using a variable delay time ranging from 3.5 ms to 900 ms and a 2-ms Gaussian radiofrequency excitation pulse to generate a free induction decay, which was repeated 32 times during a single breath-hold. The resulting ^{129}Xe spectra were processed using code written in MATLAB.

Safety monitoring and xenon dosing

Hyperpolarized ^{129}Xe gas was administered in the presence of a registered nurse or physician. The subject heart rate (beats per minute, or bpm) and blood oxygenation (SpO_2) were monitored via an MR-compatible pulse oximeter (model 865353 MRI Patient Monitor; InVivo, Orlando, FL). Subject resting baseline heart rate and SpO_2 were recorded prior to inhaling ^{129}Xe, and heart rate and SpO_2 were monitored for 2 min post-inhalation for every dose of ^{129}Xe gas. We recorded nadir SpO_2 (i.e. the lowest blood oxygenation post inhalation), subject heart rate at the time of the SpO_2 nadir, and the duration of the SpO_2 nadir. Immediately following each dose, the gas administrator performed a brief assessment to evaluate the central nervous system effects of hyperpolarized ^{129}Xe. In this assessment, the child was asked to describe any sensations such as dizziness, light-headedness, numbness or euphoria. Prior to additional doses of ^{129}Xe gas, the child breathed room air for at least 2 min. We administered a maximum of three ^{129}Xe doses per child, including the calibration dose. Adverse events were assessed at the time of imaging and during two follow-up phone calls at day 1 and day 30 (range ±7 days) post imaging.

As an initial test of tolerability and feasibility, the first five healthy volunteers (subjects HV-1 through HV-5) were imaged with a half-dose of gas (approximately equal to one-twelfth of their predicted TLC volume as calculated from the ATS plethysmography-based guidelines for pediatrics [64, 65]). Briefly, TLC is given by the equations $TLC\,(L) = 9.96 \times h^{2.5698} \times 10^{-6}$ for boys and $TLC\,(L) = 9.17 \times h^{2.5755} \times 10^{-6}$ for girls, where h is the subject's height in centimeters. Predicted TLC values were used (as opposed to performing plethysmography in each individual subject), because plethysmography overestimates functional volumes in cases of significant airway obstruction and air trapping [66] — a specific concern for children with cystic fibrosis. The remaining healthy volunteers (HV-6 through HV-17) and all children with CF received a full imaging dose of up to one-sixth of the predicted TLC, with a maximum dose of 1 liter. In subsequent text, these larger-volume doses are referred to as full doses to distinguish them from the initial one-twelfth TLC doses (half-doses) and the calibration doses.

Statistical analysis

Nadir SpO_2 and heart rate at the time of SpO_2 nadir were compared to resting baseline values to determine changes post inhalation of xenon gas. Baseline SpO_2 and heart rate were also compared to SpO_2 and heart rate at 2-min post inhalation. For these comparisons, two-sided paired t-tests with unequal variance were used to determine statistically significant (P-value≤0.05) changes in heart rate and SpO_2. For the purposes of comparing children with CF and healthy controls, we performed Welch two-sample t-tests with 95% confidence interval. We used Bland–Altman analysis to evaluate the difference between the SpO_2 nadirs for the calibration and imaging doses.

Results

Tolerability and physiological monitoring

The first five healthy children received and tolerated a half-dose of gas, or 1/12 of the predicted TLC (HV-1 through HV-5), and no child withdrew from the study. Table 2

summarizes the changes in SpO_2 and heart rate for these children during the ^{129}Xe gas administration (subject HV-1 was excluded from the analysis because nadir SpO_2 and heart rate at the SpO_2 nadir were not captured). The SpO_2 nadir post inhalation was −2.5 ± 2.4% (mean ± standard deviation) for the calibration dose and −4.3 ± 4.6% for the imaging dose; however this drop was not significantly different from the resting baseline value (P=0.13 and P=0.16 for the calibration and imaging doses, respectively). For the calibration dose, there was no significant difference in SpO_2 at 2 minutes post inhalation relative to baseline (P=0.22). For the imaging dose (a half-dose), subject SpO_2 at 2 minutes post inhalation was lower compared to baseline (97.4±1.3%, P=0.034); however the change (a reduction of 1% below baseline) was not physiologically significant. Table 2 also summarizes changes in heart rate for these five children throughout the ^{129}Xe imaging; there were no significant changes in heart rate for any time-point comparison for either the calibration or imaging doses, with P-values ≥ 0.22.

After reviewing the safety data and adverse events for the initial five healthy volunteers, full imaging doses of gas were administered to the remaining controls (HV-6 through HV-17) and all children with CF. Again, no children withdrew from this stage of the study and no medical intervention was required at any time for any child. Table 3 summarizes the changes in SpO_2 during the gas administration. Relative to baseline, the average change in SpO_2 was −2.9 ± 2.9% (P≤0.001) for the calibration doses and −6.0 ± 7.2% (P≤0.001) for the imaging doses. Although there were no significant differences in SpO_2 at 2 minutes post inhalation relative to baseline, a slight trend toward increased values was observed (calibration dose at P=0.069 and imaging dose at P=0.11). Additionally, of the 50 total doses administered to these 23 children, either no change or an increase in SpO_2 was reported for six doses, likely representing normal physiological variability in SpO_2.

Figure 1 is a Bland–Altman plot comparing the magnitudes of the SpO_2 nadirs for the calibration and imaging doses for all three groups of subjects (i.e. controls with half-dosing, controls with full-dosing, and children with CF). For all doses of gas for all children, the mean difference in the SpO_2 nadirs between the imaging and calibration doses was −2.7 ± 7.7%, meaning that the SpO_2 nadir for the imaging dose was slightly larger. For subject CF-7, the SpO_2 nadir for the calibration dose was only −1%; however the nadir SpO_2 for the imaging dose was −29% (nadir of 67%, with a baseline of 96%). This nadir spontaneously resolved, and the SpO_2 quickly recovered without intervention (97% at 2 minutes post inhalation).

Table 4 shows the heart rate changes at the same four time-points for these children. There were no significant changes in subject heart rate throughout the calibration dose (P-values ≥ 0.46). For the imaging dose, there was a significant elevation in heart rate (captured at the time of the SpO_2 nadir) to 83.5±16.6 bpm (P=0.021 relative to a baseline value of 76.9±13.1 bpm), which returned to resting baseline by 2 minutes post inhalation (P=0.35).

Control- versus CF-group comparisons

For the purposes of comparing changes in vital signs between children with CF and healthy controls, only the children who received full doses of gas were considered (n=23, subjects HV-6 through HV-17 and all children with CF). There were no significant differences in age

(P=0.36), weight (P=0.74), height (P=0.40) or forced expiratory volume in 1 second (FEV_1) predicted (P=0.44) between these controls and the children with CF. The SpO_2 nadir was not significantly different between controls and children with CF for the calibration dose (−3.0 ± 2.6%, and −2.8 ± 3.3% for the controls and children with CF, respectively; P=0.89). Likewise, there was no significant difference in the SpO_2 nadir for the imaging doses between the control and CF groups (−4.6 ± 4.1% and −7.4 ± 9.4%, respectively; P=0.35).

Following inhalation of the calibration dose, all control subjects except HV-9 experienced a nadir in SpO_2 (P≤0.01 versus baseline), but SpO_2 returned to baseline within 2 minutes post inhalation (P=0.21 versus baseline). Similar SpO_2 changes were observed in the children with CF (P=0.017 for the SpO_2 nadir; P=0.10 at 2 minutes post inhalation). Prior to inhaling a full imaging dose of gas, control subjects had a baseline SpO_2 of 98.5±1.2%, which was significantly reduced following inhalation (nadir of 93.9±4.0%, P=≤0.001). At 2 minutes post inhalation, SpO_2 remained slightly decreased in these children (97.5±1.7%, P=0.024 relative to baseline), but this change was not physiologically relevant. Children with CF experienced a similarly significant SpO_2 nadir relative to baseline (97.3±1.6% at baseline, 89.9±9.8% at the nadir, P=0.015). However, SpO_2 returned to baseline values by 2 minutes post inhalation (97.3±1.8%, P=1.0 compared to baseline).

For the calibration doses, there was no significant change in heart rate (i.e. the difference between resting baseline and the heart rate recorded at the SpO_2 nadir post inhalation), with the mean for control subjects being +0.8 ± 9.4 bpm compared to +2.4 ± 10.4 bpm for the children with CF (P=0.70). Likewise, for the imaging doses of gas, there was no significant change in mean heart rate for the children with CF (+5.5 ± 14 bpm) or the controls (+7.5 ± 14.2 bpm; P=0.72). There were also no statistically significant changes in heart rate for any time-point comparison for the control group (P≥0.070). However there was a trend toward significance for an elevation in heart rate at the time of the SpO_2 nadir in children with CF (P≥0.18) in both imaging and calibration doses of gas.

Neurological symptoms and adverse events

None of the half-dose cohort (one-twelfth TLC) reported central nervous system effects, while in general all children receiving the full dose of gas (one-sixth TLC) experienced central nervous system effects to some degree. However all side effects were mild and consistent with the sub-anesthetic properties of xenon (e.g., tingling, dizziness, euphoria) at these relatively low alveolar xenon concentrations. Moreover, all side effects resolved quickly (<30 s) and spontaneously after breathing room air for 2 minutes. In total, four adverse events were reported, but none was serious, and all were determined to be unrelated to the study. At the day 1 follow-up phone call, the parent of subject HV-5 reported that the child ate food too quickly and vomited later in the day of the imaging procedure. However because of the child's reported history of this behavior, this event was deemed unrelated to the study. Three of the four adverse events were reported at the day 30 follow-up phone call: cough (subject CF-2), influenza B (CF-1), and upper respiratory tract infection (CF-3), and each of the three cases reported a decrease in pulmonary function tests. Given the common susceptibility of children with CF to decreases in pulmonary function, these adverse events were also considered to be unrelated to the study.

Pediatric ^{129}Xe MRI feasibility

All children were able to perform the up to 16 s breath-hold maneuver required for MR studies. Moreover, diagnostically meaningful ^{129}Xe MR images were successfully obtained from all children. Illustrative examples of the most promising of these potential ^{129}Xe MR applications (i.e. spectroscopy, diffusion-weighted MRI, and ventilation imaging) are demonstrated in Figs. 2, 3 and 4.

Discussion

Safety and tolerability

In this study we examined the safety, tolerability and feasibility of hyperpolarized ^{129}Xe gas as an inhaled contrast agent for pulmonary MR of children with and without lung disease (cystic fibrosis). Although most children did experience a statistically significant nadir in SpO_2 after inhaling the ^{129}Xe gas, it is important to note that these changes were clinically insignificant and fully consistent with expectations from previous hyperpolarized-gas MRI studies [52, 53, 67]. In general an increase in heart rate was noted at the time of the SpO_2 nadir; however this increase was only statistically significant for one comparison (i.e. the aggregate analysis for children receiving the full-volume imaging dose of gas, P=0.021). Moreover these changes in SpO_2 and heart rate were small and transient and resolved quickly without medical intervention, within 2 minutes of normal breathing. At the 2-minute recovery time-point, subject SpO_2 remained decreased relative to baseline for one comparison (controls with full imaging doses of gas, P=0.024), but this decrease was not clinically significant (approximately a 1% change from 98.5% at baseline to 97.5% at 2 minutes post inhalation). For the aggregate analysis of children receiving the full imaging dose of gas, there was a mean increase in heart rate of 6.6 bpm after gas inhalation; while this increase was statistically significant, it was clinically insignificant and subject heart rate returned to resting baseline values within 2 minutes.

Our results were in good agreement with previous assessments of ^{129}Xe MRI safety in adults [52, 53]. In a phase 1 clinical trial of ^{129}Xe MRI conducted at Duke University Medical Center [52] involving 44 adults who inhaled up to five 1-liter doses of xenon gas, no significant changes in vital signs were observed within 10 minutes post inhalation (note, the presence of a nadir SpO_2 was not explicitly examined in this study). No subjects withdrew from that study or experienced any serious or severe adverse events. Although most subjects experienced transient symptoms related to the known anesthetic properties of xenon, all symptoms resolved without clinical intervention in 1.6±0.9 min [52]. In a second study of ^{129}Xe tolerability in adults, conducted at Robarts Research Institute [53], 33 adults were imaged with 0.5 l ^{129}Xe gas mixed with 0.5 l ^{4}He. All subjects tolerated these doses well, no subjects withdrew from the study, and no severe adverse events were observed. Two subjects reported mild adverse events (light-headedness), likely related to xenon administration, but these events resolved within 2 minutes and without intervention. Similar to our results, they reported statistically significant changes in SpO_2 and heart rate immediately post inhalation. However these changes were also clinically insignificant and returned to resting baseline within 1 minute and without intervention [53].

Because ^{129}Xe MRI was performed during a short breath-hold using sub-anesthetic doses of Xe gas, all central nervous system effects experienced by the children in this study were mild and resolved spontaneously with normal breathing of room air. Note, in earlier assessments of hyperpolarized ^{129}Xe safety in adults [52, 53], central nervous system effects were described in great detail, with subjects differentiating between nuanced sensations such as euphoria and light-headedness. However, we anticipated that making similar distinctions would be challenging for some younger pediatric subjects, thus we combined central nervous system effects into a single category.

The Xe dosing strategy of one-sixth of the predicted TLC dose resulted in an alveolar concentration ~17% for a single breath as compared to ~30% concentration sustained over minutes for Xe-enhanced CT [56] and ~63% to initiate anesthesia [50]. Even if the predicted TLC was overestimated by 30%, the alveolar concentration would only have reached 24% for a single breath. The SpO_2 nadir was larger for the full imaging doses of ^{129}Xe gas relative to the calibration doses for most children, which is likely related to the longer anoxic breath-hold duration (i.e. ~2 s and up to 16 s for the calibration and imaging doses, respectively). For all children except subject CF-7, the magnitude of the SpO_2 nadirs fell within the 95% confidence interval, suggesting the change in SpO_2 was not related to the volume of xenon gas inhaled but rather to the anoxic breath-hold itself (i.e. the effects of the Xe gas are not likely to manifest during a single 16-s breath-hold, as opposed to minutes-long exposure at high concentrations for anesthesia). While ^{129}Xe MRI generally was well tolerated by all children, one child with CF (CF-7) had an SpO_2 drop from 96% to 67% during the imaging dose breath-hold, which quickly recovered to baseline without intervention (97% at 2 min post inhalation). This child did not clearly differ from other children in terms of age or lung function (FEV_1=102%), highlighting the value of SpO_2 motoring during the anoxic xenon breath-holds.

For this initial assessment of ^{129}Xe MRI, our cohort comprised both healthy children and children with CF who had mild to moderate lung disease. CF was chosen for this initial study (as opposed to asthma, for example) because of its known genetic etiology. While no significant differences in vital sign changes were observed between these groups, it is possible that children with other pulmonary diseases or with more severe disease may respond differently to the anoxic ^{129}Xe gas inhalation. Children with more severe disease might also have difficulty performing the 16-s breath-hold employed for our ^{129}Xe imaging studies. However the use of more efficient imaging sequences (e.g., acquisitions with spiral k-space trajectories [68, 69]) that enable faster imaging and reduced breath-hold durations and the addition of O_2 to the inhaled gas mixture (via a second bag to mitigate T_1 relaxation [45]) would mitigate the majority of these obstacles.

Compliance with the inhalation maneuvers

Compliance with breathing maneuvers can be challenging for children compared to adults. To address this issue, the team member responsible for ^{129}Xe gas administration worked to build a good rapport with the children, which helped to avoid complications and increased compliance with imaging. Children performed a practice breath-hold with a bag of air during a conventional ^{1}H gradient-echo sequence (with the same duration as the ^{129}Xe scan)

to acclimate to the scanner environment. Practice breath-holds were repeated until a child could comfortably perform the maneuver before Xe was administered. Typically only one to two practice attempts were required to achieve full compliance during the ^{129}Xe scans.

Feasibility of pediatric studies with hyperpolarized ^{129}Xe

Hyperpolarized ^{129}Xe MRI has the potential to provide unique regional insights into gas exchange, lung microstructure and ventilation at little or no risk to the child, even in younger children with significant underlying lung disease. A ^{129}Xe magnetic resonance spectrum for subject HV-17 is presented in Fig. 2. Although the majority of the ^{129}Xe MR signal originates from gaseous ^{129}Xe in the alveolar spaces (by convention, reference to 0 ppm), two small peaks are observed near ~200 ppm, demonstrating the high sensitivity of the ^{129}Xe resonance frequency to differences in chemical environment. Previously, these unique physical and MR properties of ^{129}Xe (i.e. the ability to dissolve in lung tissues and produce resonances specific to red blood cells and barrier tissues) have been exploited to visualized dynamic gas uptake and regionally impaired exchange in adults [11, 45, 46, 48, 49].

In apparent diffusion coefficient (ADC) maps obtained from diffusion-weighted ^{129}Xe images (Fig. 3), the mean ^{129}Xe ADC was 0.029±0.01 cm^2/s for HV-15 and 0.031±0.02 cm^2/s for HV-3. Notably, these mean ADC values are smaller than those previously reported for healthy adults (~0.04 cm^2/s [70]). Consistent with previous observation using hyperpolarized ^{3}He, these differences likely arise from the smaller alveoli present in these young subjects and demonstrates the high sensitivity of ^{129}Xe to even minute differences in alveolar microstructure [24].

As expected from ^{129}Xe ventilation imaging of healthy adults [15, 71, 72], the control subject in Fig. 4 displayed qualitatively uniform signal intensity throughout the lungs. The variability that is observed, aside from gravitationally dependent gradients in ventilation, results from shading caused by imperfect coil uniformity. In contrast, the ventilation pattern of the child with CF is highly heterogeneous and contains regions of little to no ^{129}Xe signal despite this child having a normal FEV_1, which was higher than that of the control. These so-called ventilation defects are well-known features of hyperpolarized-gas lung images from individuals with various lung diseases and are indicative of regionally impaired ventilation [10, 71].

Conclusion

We report the assessment of the safety, tolerability and feasibility of ^{129}Xe MRI in a small cohort of children with and without lung disease. Our data indicate that ^{129}Xe is a safe and easily tolerated inhaled contrast agent for pulmonary imaging, paving the way for studies of other pulmonary diseases as well as larger-scale clinical trials with pediatric subjects. ^{129}Xe MRI has a well-established track record in imaging adult lung disease and has repeatedly demonstrated its utility in quantifying regional ventilation and acinar microstructural parameters noninvasively and without the use of ionizing radiation. In particular, applying ^{129}Xe MRI techniques to pediatric lung disease might provide a means to quantify

subtle longitudinal changes in gas exchange, ventilation and alveolar microstructure associated with pulmonary disease progression and to assess response to treatment.

Acknowledgments

The authors would like to acknowledge Bastiaan Driehuys, Leslie Korbee, Jenny Jeffries, Lisa McCord, Colleen Murphy and Jeanne Dahlquist for regulatory assistance; Laurie Vanderah, Beth Decker and Emily Bell for subject monitoring; Matthew Lanier, Brynne Williams and Lacey Haas for subject scanning; Dan Dwyer of Teleflex Inc. for the gift of the custom gas-delivery mouthpieces; and Matthew Freeman, Nara Higano, Jim Wild, Charles Dumoulin and the CCHMC IRC Coil Engineering Lab for technical assistance.

This work was supported by the National Institutes of Health (T32HL007752, R01HL116226), Cystic Fibrosis Foundation (CLANCY 15R0), and University of Cincinnati, Center for Clinical and Translational Science and Training (T1 Core).

References

1. Mugler JP 3rd, Driehuys B, Brookeman JR, et al. MR imaging and spectroscopy using hyperpolarized ^{129}Xe gas: preliminary human results. Magn Reson Med. 1997; 37:809–815. [PubMed: 9178229]
2. Black RD, Middleton HL, Cates GD, et al. In vivo He-3 MR images of guinea pig lungs. Radiology. 1996; 199:867–870. [PubMed: 8638019]
3. MacFall JR, Charles HC, Black RD, et al. Human lung air spaces: potential for MR imaging with hyperpolarized He-3. Radiology. 1996; 200:553–558. [PubMed: 8685356]
4. Spector ZZ, Emami K, Fischer MC, et al. Quantitative assessment of emphysema using hyperpolarized 3He magnetic resonance imaging. Magn Reson Med. 2005; 53:1341–1346. [PubMed: 15906306]
5. Emami K, Kadlecek SJ, Woodburn JM, et al. Improved technique for measurement of regional fractional ventilation by hyperpolarized 3He MRI. Magn Reson Med. 2010; 63:137–150. [PubMed: 19877277]
6. Yablonskiy DA, Sukstanskii AL, Leawoods JC, et al. Quantitative in vivo assessment of lung microstructure at the alveolar level with hyperpolarized He-3 diffusion MRI. Proc Natl Acad Sci USA. 2002; 99:3111–3116. [PubMed: 11867733]
7. Saam BT, Yablonskiy DA, Kodibagkar VD, et al. MR imaging of diffusion of He-3 gas in healthy and diseased lungs. Magn Reson Med. 2000; 44:174–179. [PubMed: 10918314]
8. Wang W, Nguyen NM, Yablonskiy DA, et al. Imaging lung microstructure in mice with hyperpolarized He-3 diffusion MRI. Magn Reson Med. 2011; 65:620–626. [PubMed: 21337400]
9. Yablonskiy DA, Sukstanskii AL, Quirk JD, et al. Probing lung microstructure with hyperpolarized noble gas diffusion MRI: theoretical models and experimental results. Magn Reson Med. 2014; 71:486. [PubMed: 23554008]
10. Kirby M, Svenningsen S, Kanhere N, et al. Pulmonary ventilation visualized using hyperpolarized helium-3 and xenon-129 magnetic resonance imaging: differences in COPD and relationship to emphysema. J Appl Physiol. 1985; 114:707–715.
11. Dregely I, Mugler JP III, Ruset IC, et al. Hyperpolarized xenon-129 gas-exchange imaging of lung microstructure: first case studies in subjects with obstructive lung disease. J Magn Reson Imaging. 2011; 33:1052–1062. [PubMed: 21509861]
12. McMahon CJ, Dodd JD, Hill C, et al. Hyperpolarized 3helium magnetic resonance ventilation imaging of the lung in cystic fibrosis: comparison with high resolution CT and spirometry. Eur Radiol. 2006; 16:2483–2490. [PubMed: 16871384]
13. Donnelly LF, MacFall JR, McAdams HP, et al. Cystic fibrosis: combined hyperpolarized 3He-enhanced and conventional proton MR imaging in the lung — preliminary observations. Radiology. 1999; 212:885–889. [PubMed: 10478261]
14. de Lange EE, Altes TA, Patrie JT, et al. Evaluation of asthma with hyperpolarized helium-3 MRI: correlation with clinical severity and spirometry. Chest. 2006; 130:1055–1062. [PubMed: 17035438]

15. Altes TA, Powers PL, Knight-Scott J, et al. Hyperpolarized He-3 MR lung ventilation imaging in asthmatics: preliminary findings. J Magn Reson Imaging. 2001; 13:378–384. [PubMed: 11241810]
16. Thomen RP, Sheshadri A, Quirk JD, et al. Regional ventilation changes in severe asthma after bronchial thermoplasty with (3)He MR imaging and CT. Radiology. 2015; 274:250–259. [PubMed: 25144646]
17. Appelt S, Baranga AB, Erickson CJ, et al. Theory of spin-exchange optical pumping of He-3 and Xe-129. Phys Rev A. 1998; 58:1412–1439.
18. Walker TG, Happer W. Spin-exchange optical pumping of noble-gas nuclei. Rev Mod Phys. 1997; 69:629–642.
19. Fain S, Schiebler ML, McCormack DG, Parraga G. Imaging of lung function using hyperpolarized helium-3 magnetic resonance imaging: review of current and emerging translational methods and applications. J Magn Reson Imaging. 2010; 32:1398–1408. [PubMed: 21105144]
20. Mugler JP 3rd, Altes TA. Hyperpolarized 129Xe MRI of the human lung. J Magn Reson Imaging. 2013; 37:313–331. [PubMed: 23355432]
21. Lilburn DM, Pavlovskaya GE, Meersmann T. Perspectives of hyperpolarized noble gas MRI beyond 3He. J Magn Reson. 2013; 229:173–186. [PubMed: 23290627]
22. Walkup LL, Woods JC. Translational applications of hyperpolarized 3He and 129Xe. NMR Biomed. 2014; 27:1429–1438. [PubMed: 24953709]
23. Altes TA, de Lange EE. Applications of hyperpolarized helium-3 gas magnetic resonance imaging in pediatric lung disease. TMRI. 2003; 14:231–236. [PubMed: 12973130]
24. Altes TA, Mata J, de Lange EE, et al. Assessment of lung development using hyperpolarized helium-3 diffusion MR imaging. JMRI. 2006; 24:1277–1283. [PubMed: 17096396]
25. Altes TA, Mata J, Froh DK, et al. Abnormalities of lung structure in children with brochopulmonary dysplasia as assessed by diffusion hyperpolarized helium-3 MRI. Proc Intl Soc Magn Reson Med. 2006; 14:86.
26. Kirby M, Coxson HO, Parraga G. Pulmonary functional magnetic resonance imaging for paediatric lung disease. Paediatr Respir Rev. 2013; 14:180–189. [PubMed: 23522599]
27. van Beek EJ, Hill C, Woodhouse N, et al. Assessment of lung disease in children with cystic fibrosis using hyperpolarized 3-Helium MRI: comparison with Shwachman score, Chrispin-Norman score and spirometry. Eur Radiol. 2007; 17:1018–1024. [PubMed: 16941089]
28. Woodhouse N, Wild JM, van Beek EJ, et al. Assessment of hyperpolarized 3He lung MRI for regional evaluation of interventional therapy: a pilot study in pediatric cystic fibrosis. JMRI. 2009; 30:981–988. [PubMed: 19856418]
29. Koumellis P, van Beek EJ, Woodhouse N, et al. Quantitative analysis of regional airways obstruction using dynamic hyperpolarized 3He MRI-preliminary results in children with cystic fibrosis. J Magn Reson Imaging. 2005; 22:420–426. [PubMed: 16104046]
30. McMahon CJ, Dodd JD, Hill C, et al. Hyperpolarized (3)helium magnetic resonance ventilation imaging of the lung in cystic fibrosis: comparison with high resolution CT and spirometry. Eur Radiol. 2006; 16:2483–2490. [PubMed: 16871384]
31. Sun Y, O'Sullivan BP, Roche JP, et al. Using hyperpolarized 3He MRI to evaluate treatment efficacy in cystic fibrosis patients. J Magn Reson Imaging. 2011; 34:1206–1211. [PubMed: 21932361]
32. Cadman RV, Lemanske RF, Evans MD, et al. Pulmonary He-3 magnetic resonance imaging of childhood asthma. J Allergy Clin Immunol. 2013; 131:369–376. [PubMed: 23246019]
33. de Lange EE, Altes TA, Patrie JT, et al. The variability of regional airflow obstruction within the lungs of patients with asthma: assessment with hyperpolarized helium-3 magnetic resonance imaging. J Allergy Clin Immunol. 2007; 119:1072–1078. [PubMed: 17353032]
34. Narayanan M, Owers-Bradley J, Beardsmore CS, et al. Alveolarization continues during childhood and adolescence: new evidence from helium-3 magnetic resonance. Am J Respir Crit Care Med. 2012; 185:186–191. [PubMed: 22071328]
35. Narayanan M, Beardsmore CS, Owers-Bradley J, et al. Catch-up alveolarization in ex-preterm children: evidence from (3)He magnetic resonance. Am J Respir Crit Care Med. 2013; 187:1104–1109. [PubMed: 23491406]

36. Anglister J, Grzesiek S, Ren H, et al. Isotope-edited multidimensional NMR of calcineurin B in the presence of the non-deuterated detergent CHAPS. J Biomol NMR. 1993; 3:121–126. [PubMed: 8383554]
37. Nikolaou P, Coffey AM, Walkup LL, et al. XeNA: An automated 'open-source' (129)Xe hyperpolarizer for clinical use. Magn Reson Imaging. 2014; 32:541–550. [PubMed: 24631715]
38. Nikolaou P, Coffey AM, Walkup LL, et al. A 3D-printed high power nuclear spin polarizer. J Am Chem Soc. 2014; 136:1636–1642. [PubMed: 24400919]
39. Korchak SE, Kilian W, Mitschang L. Configuration and performance of a mobile (129)Xe polarizer. Appl Magn Reson. 2013; 44:65–80. [PubMed: 23349565]
40. Stewart NJ, Norquay G, Griffiths PD, Wild JM. Feasibility of human lung ventilation imaging using highly polarized naturally abundant xenon and optimized three-dimensional steady-state free precession. Magn Reson Med. 2015; 74:346–352. [PubMed: 25916276]
41. Hersman FW, Ruset IC, Ketel S, et al. Large production system for hyperpolarized 129Xe for human lung imaging studies. Acad Radiol. 2008; 15:683–692. [PubMed: 18486005]
42. Kirby M, Svenningsen S, Owrangi A, et al. Hyperpolarized 3He and 129Xe MR imaging in healthy volunteers and patients with chronic obstructive pulmonary disease. Radiology. 2012; 265:600–610. [PubMed: 22952383]
43. Patz S, Hersman FW, Muradian I, et al. Hyperpolarized (129)Xe MRI: a viable functional lung imaging modality? Eur J Radiol. 2007; 64:335–344. [PubMed: 17890035]
44. Chen RY, Fan FC, Kim S, et al. Tissue-blood partition coefficient for xenon: temperature and hematocrit dependence. J Appl Physiol Respir Environ Exerc Physiol. 1980; 49:178–183. [PubMed: 7400000]
45. Mugler JP 3rd, Altes TA, Ruset IC, et al. Simultaneous magnetic resonance imaging of ventilation distribution and gas uptake in the human lung using hyperpolarized xenon-129. Proc Natl Acad Sci USA. 2010; 107:21707–21712. [PubMed: 21098267]
46. Cleveland ZI, Cofer GP, Metz G, et al. Hyperpolarized Xe MR imaging of alveolar gas uptake in humans. PLoS One. 2010; 5:e12192. [PubMed: 20808950]
47. Kaushik SS, Freeman MS, Cleveland ZI, et al. Probing the regional distribution of pulmonary gas exchange through single-breath gas- and dissolved-phase 129Xe MR imaging. J Appl Physiol (1985). 2013; 115:850–860. [PubMed: 23845983]
48. Qing K, Mugler JP 3rd, Altes TA, et al. Assessment of lung function in asthma and COPD using hyperpolarized 129Xe chemical shift saturation recovery spectroscopy and dissolved-phase MRI. NMR Biomed. 2014; 27:1490–1501. [PubMed: 25146558]
49. Ruppert K, Altes TA, Mata JF, et al. Detecting pulmonary capillary blood pulsations using hyperpolarized xenon-129 chemical shift saturation recovery (CSSR) MR spectroscopy. Magn Reson Med. 2016; 75:1771–1780. [PubMed: 26017009]
50. Nakata Y, Goto T, Ishiguro Y, et al. Minimum alveolar concentration (MAC) of xenon with sevoflurane in humans. Anesthesiology. 2001; 94:611–614. [PubMed: 11379681]
51. Sanders RD, Franks NP, Maze M. Xenon: no stranger to anaesthesia. Br J Anaesth. 2003; 91:709–717. [PubMed: 14570795]
52. Driehuys B, Martinez-Jimenez S, Cleveland ZI, et al. Chronic obstructive pulmonary disease: safety and tolerability of hyperpolarized Xe-129 MR imaging in healthy volunteers and patients. Radiology. 2012; 262:279–289. [PubMed: 22056683]
53. Shukla Y, Wheatley A, Kirby M, et al. Hyperpolarized 129Xe magnetic resonance imaging: tolerability in healthy volunteers and subjects with pulmonary disease. Acad Radiol. 2012; 19:941–951. [PubMed: 22591724]
54. Chae EJ, Seo JB, Goo HW, et al. Xenon ventilation CT with a dual-energy technique of dual-source CT: initial experience. Radiology. 2008; 248:615–624. [PubMed: 18641254]
55. Goo HW, Chae EJ, Seo JB, Hong SJ. Xenon ventilation CT using a dual-source dual-energy technique: dynamic ventilation abnormality in a child with bronchial atresia. Pediatr Radiol. 2008; 38:1113–1116. [PubMed: 18542942]
56. Goo HW, Yang DH, Hong SJ, et al. Xenon ventilation CT using dual-source and dual-energy technique in children with bronchiolitis obliterans: correlation of xenon and CT density values with pulmonary function test results. Pediatr Radiol. 2010; 40:1490–1497. [PubMed: 20411254]

57. Miller MR, Hankinson J, Brusasco V, et al. Standardisation of spirometry. Eur Respir J. 2005; 26:319–338. [PubMed: 16055882]
58. Farrell PM, Rosenstein BJ, White TB, et al. Guidelines for diagnosis of cystic fibrosis in newborns through older adults: Cystic Fibrosis Foundation consensus report. J Pediatr. 2008; 153:S4–S14. [PubMed: 18639722]
59. Walkup, L.; Higano, N.; Ellis-Caleo, T., et al. Scaling-up an 'open-source' 129Xe hyperpolarizer for human pulmonary imaging applications. Presented at the Experimental Nuclear Magnetic Resonance Conference; Boston. 2014.
60. Walkup, LL.; Thomen, RP.; Higano, NS., et al. Initial experience performing hyperpolarized 129Xe MRI in young, pediatric subjects using a homebuilt Xe polarizer. Presented at the Experimental Nuclear Magnetic Resonance Conference; Pittsburgh. 2016.
61. Loew W, Thomen R, Pratt R, et al. A volume saddle coil for hyperpolarized 129Xe lung imaging. Proc Intl Soc Magn Reson Med. 2015; 23:1507.
62. Miller GW, Altes TA, Brookeman JR, et al. Hyperpolarized 3He lung ventilation imaging with B1-inhomogeneity correction in a single breath-hold scan. Magma. 2004; 16:218–226. [PubMed: 15108030]
63. Yablonskiy DA, Sukstanskii AL, Quirk JD. Diffusion lung imaging with hyperpolarized gas MRI. NMR in Biomed. 2015; doi: 10.1002/nbm.3448
64. Stocks J, Quanjer PH. Reference values for residual volume, functional residual capacity and total lung capacity. ATS workshop on lung volume measurements. Official statement of the European Respiratory Society. Eur Respir J. 1995; 8:492–506. [PubMed: 7789503]
65. Zapletal A, Paul T, Samanek M. Significance of contemporary methods of lung function testing for the detection of airway obstruction in children and adolescents (author's transl). Z Erkr Atmungsorgane. 1977; 149:343–371. [PubMed: 613549]
66. West, JB. Respiratory physiology: the essentials. 9. Lippincott Williams & Wilkins; Baltimore: 2012.
67. Lutey BA, Lefrak SS, Woods JC, et al. Hyperpolarized 3He MR imaging: physiologic monitoring observations and safety considerations in 100 consecutive subjects. Radiology. 2008; 248:655–661. [PubMed: 18641256]
68. Salerno M, Altes TA, Brookeman JR, et al. Rapid hyperpolarized 3He diffusion MRI of healthy and emphysematous human lungs using an optimized interleaved-spiral pulse sequence. J Magn Reson Imaging. 2003; 17:581–588. [PubMed: 12720268]
69. Salerno M, Altes TA, Brookeman JR, et al. Dynamic spiral MRI of pulmonary gas flow using hyperpolarized (3)He: preliminary studies in healthy and diseased lungs. Magn Reson Med. 2001; 46:667–677. [PubMed: 11590642]
70. Kaushik SS, Cleveland ZI, Cofer GP, et al. Diffusion-weighted hyperpolarized 129Xe MRI in healthy volunteers and subjects with chronic obstructive pulmonary disease. Magn Reson Med. 2011; 65:1154–1165. [PubMed: 21413080]
71. Virgincar RS, Cleveland ZI, Kaushik SS, et al. Quantitative analysis of hyperpolarized 129Xe ventilation imaging in healthy volunteers and subjects with chronic obstructive pulmonary disease. NMR Biomed. 2013; 26:424–435. [PubMed: 23065808]
72. Kauczor HU, Hofmann D, Kreitner KF, et al. Normal and abnormal pulmonary ventilation: visualization at hyperpolarized He-3 MR imaging. Radiology. 1996; 201:564–568. [PubMed: 8888259]

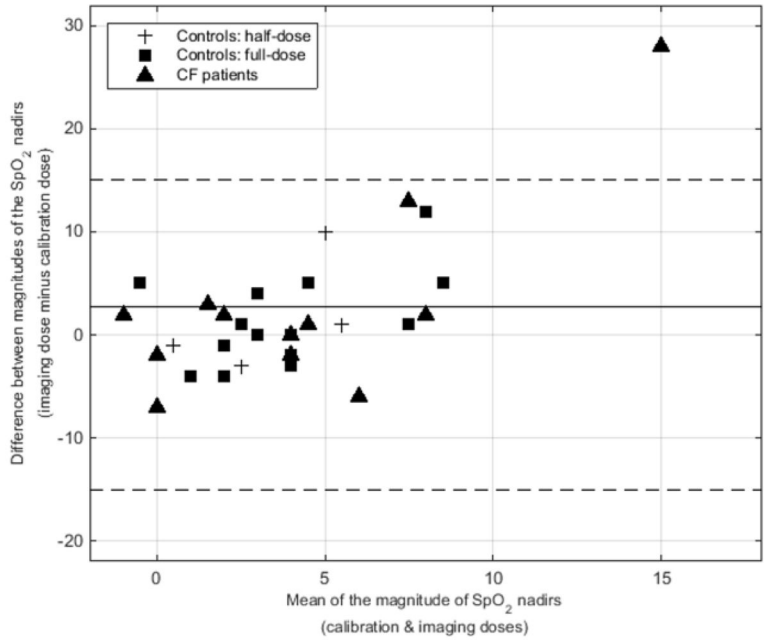

Fig. 1.

Bland–Altman plot shows a comparison of the magnitude of the SpO_2 nadirs for the calibration and imaging doses for all three subject groups (controls with half-doses of hyperpolarized gas, controls with full doses, and children with cystic fibrosis, who all received full doses. Across all subjects and all doses, the mean difference in SpO_2 nadir for the imaging and calibration doses was −2.7±7.7% (*solid line*; magnitude is plotted). Note the 95% confidence intervals (*dashed lines*). *CF* cystic fibrosis

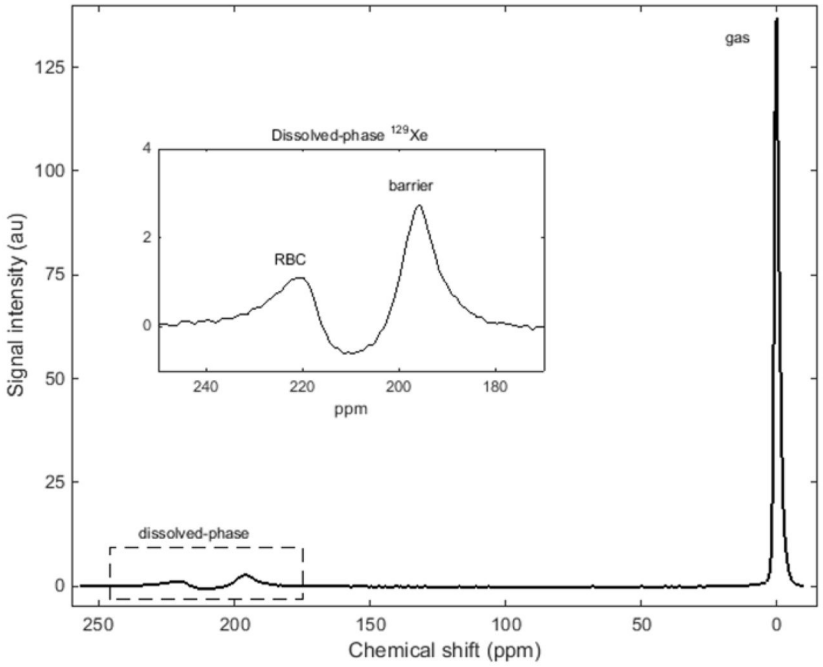

Fig. 2.

^{129}Xe MR spectrum from a healthy 16-year-old girl, subject HV-17. Three spectral peaks are observed: the bulk gas-phase peak (0 ppm) and two dissolved-phase peaks (enlarged in the inset). The other two peaks originate from hyperpolarized ^{129}Xe dissolved in the red blood cells and the barrier tissues (blood plasma and lung parenchymal tissue) peaks at ~212 ppm and ~197 ppm, respectively. *ppm* parts per minute

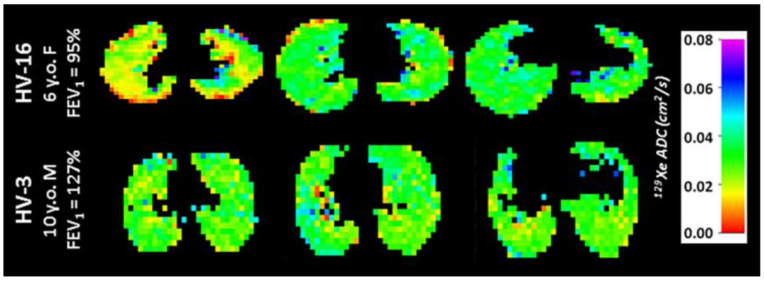

Fig. 3.

^{129}Xe apparent diffusion coefficient (ADC) maps generated via diffusion imaging in two healthy control subjects, a 6-year-old girl (HV-16, *top row*) and a 10-year-old boy (HV-3, *bottom row*) for three axial slices through the lungs. The mean ± standard deviation ^{129}Xe ADC was 0.029±0.01 cm^2/s and 0.031±0.02 cm^2/s for HV-16 and HV-3, respectively

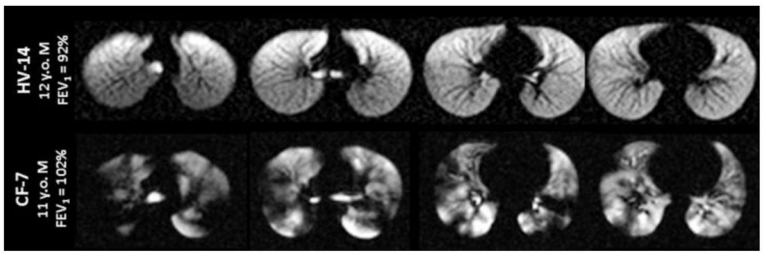

Fig. 4.

^{129}Xe ventilation images for a healthy 12-year-old boy (HV-14, *top row*) and an 11-year-old boy with cystic fibrosis (CF-7, *bottom row*). The homogeneous signal seen throughout the lungs of the healthy control indicates that all regions of the lung are well ventilated. In contrast, the hyperpolarized ^{129}Xe images of the child with cystic fibrosis display numerous regions of low signal intensity, indicating that ventilation is substantially impaired in multiple regions of the lungs

Table 1

Subject demographics and clinical information

Subject ID	Age (years)	Gender	Weight (kg)	Height (cm)	FEV_1% predicted	Predicted TLC (L)	Number of ^{129}Xe doses	CF genotype	CF pathogens[b]
Healthy volunteers (*n*=17)									
HV-1[a]	11	F	35.1	148.5	100%	3.59	2	-	-
HV-2[a]	14	M	49.1	164.6	NA	4.94	2	-	-
HV-3[a]	10	M	100.7	148.7	127%	3.81	2	-	-
HV-4[a]	10	M	39.6	138.8	91%	3.19	2	-	-
HV-5[a]	7	F	27.4	122.5	106%	2.19	2	-	-
HV-6	7	F	33	128.4	115%	2.47	2	-	-
HV-7	7	M	24.9	123.2	99%	2.35	2	-	-
HV-8	14	M	40.6	150	108%	3.89	2	-	-
HV-9	14	M	64.8	176.8	106%	5.94	2	-	-
HV-10	15	F	51.5	158.5	110%	4.25	2	-	-
HV-11	12	M	34.8	140.9	103%	3.32	2	-	-
HV-12	13	M	57.2	171.2	109%	5.47	2	-	-
HV-13	13	M	45.8	160	89%	4.60	2	-	-
HV-14	12	M	56.6	159.9	92%	4.59	2	-	-
HV-15	8	M	35.2	136	91%	3.03	2	-	-
HV-16	6	F	20.8	115.5	95%	1.88	3	-	-
HV-17	16	F	49.6	169.2	110%	5.03	3	-	-
Children with cystic fibrosis (*n*=11)									
CF-1	14	M	54.4	167	97%	5.13	2	F508Δ / F508Δ	Sa, A, Ca
CF-2	12	F	43.6	162	77%	4.50	2	F508Δ / F508Δ	A, Sp
CF-3	13	F	48.9	161	96%	4.43	2	G551D / F508Δ	-
CF-4	14	F	51.2	156	106%	4.08	2	L206W / F508Δ	Sa, Hi
CF-5	16	M	65.5	179	120%	6.13	2	F508Δ / F508Δ	Sm
CF-6	8	M	27.8	126	118%	2.49	3	F508Δ / F508Δ	Hi
CF-7	11	M	34.5	141.8	102%	3.37	3	R1066H / F508Δ	-

Subject ID	Age (years)	Gender	Weight (kg)	Height (cm)	FEV_1% predicted	Predicted TLC (L)	Number of ^{129}Xe doses	CF genotype	CF pathogens[b]
CF-8	13	F	46.5	157	114%	4.15	2	G178R / F508Δ	Hi
CF-9	15	F	43.7	159	72%	4.29	2	F508Δ / F508Δ	Sa, Pa
CF-10	11	F	40.1	152	89%	3.82	2	F508Δ / F508Δ	Sa
CF-11	11	F	34.3	147	86%	3.50	2	F508Δ / F508Δ	Pa

[a] Subject was imaged with half dose of xenon gas (1/12th predicted TLC)

[b] Pathogens grown in respiratory cultures within 1 year prior to study

A Achromobacter, *Ca* Candida albicans, *CF* cystic fibrosis, *F* female, *FEV1* forced expiratory volume in 1 second, *Hi* Haemophilus influenzae, *HV* healthy volunteers, *ID* identification, *M* male, *NA* not obtained for this child, *Pa* Pseudomonas aeruginosa, *Sa* Staphylococcus aureus, *Sm* Stenotrophomonas maltophilia, *Sp* Scedosporium prolificans, *TLC* total lung capacity

Table 2

Summary of SpO_2 and heart rate changes (mean ± standard deviation) during ^{129}Xe MRI breath-hold for children receiving the initial one-twelfth of a TLC dose of hyperpolarized gas (n=5; HV-1 through HV-5)

	Baseline	Nadir	Mean difference from baseline [95% CI][a]	*P*-value[b] (baseline vs. nadir)	2-minute recovery	Mean difference from baseline [95% CI][a]	*P*-value[b] (baseline vs. 2-minute recovery)
Calibration dose							
SpO_2 (%)	98.4 ± 1.5	96.0 ± 1.6	−2.5 [−6.3, 1.3]	0.13	98.0 ± 1.6	−0.4 [−1.8, 1.0]	0.48
HR (bpm)	75.8 ± 20.5	74.3 ± 19.0	−4.5 [−13.7, 4.7]	0.22	78.3 ± 13.8	−2.4 [−7.6, 2.8]	0.27
Imaging dose							
SpO_2 (%)	98.4 ± 1.5	94.0 ± 5.6	−4.3 [−11.6, 3.1]	0.16	97.4 ± 1.3	−1.0 [−1.9, −0.1]	0.034
HR (bpm)	72.2 ± 14.2	75.5 ± 11.0	2.0 [−16.4, 20.5]	0.75	74.2 ± 16.8	2.0 [−5.2, 9.2]	0.48

[a] Mean differences from baseline and 95% confidence intervals ([lower limit, upper limit])

[b] *P*-value ≤ 0.05 is significant

bpm beats per minute, *CI* confidence interval, *HR* heart rate, *HV* healthy volunteer, *SpO2* blood oxygenation, *TLC* total lung capacity

Table 3

Summary of mean ± standard deviation SpO_2 changes during HP ^{129}Xe imaging for children receiving full doses of xenon gas

	All children (*n*=23)	Healthy controls (*n*=12; HV-6 through HV-17)	Children with CF (*n*=11)
Calibration dose			
Baseline SpO_2 (%)	98.0 ± 1.1	98.4 ± 1.0	97.6 ± 1.2
Nadir SpO_2 (%)	95.1 ± 2.8	95.4 ± 2.4	94.8 ± 3.2
Mean difference from baseline SpO_2 (%) [95% CI]	−2.9 [−4.2, −1.7]	−3.0 −4.6, −1.4]	−2.8 [−5.0, −0.6]
P-value (baseline vs. nadir)[a]	≤0.001	≤0.01	0.017
2-minute SpO_2 (%)	97.5 ± 1.5	97.8 ± 1.8	97.3 ± 1.1
Mean difference from baseline SpO_2 (%) [95% CI]	−0.5 [−1.1, 0.0]	−0.7 [−1.8, 0.4]	−0.4 [−0.82, 0.1]
P-value (baseline vs. 2-minute)[a]	0.069	0.21	0.10
Imaging dose			
Baseline SpO_2 (%)	97.9 ± 1.4	98.5 ± 1.2	97.3 ± 1.6
Nadir SpO_2 (%)	92.0 ± 7.5	93.9 ± 4.0	89.9 ± 9.8
Mean difference from baseline SpO_2 (%) [95% CI]	−6.0 [−8.8, −3.1]	−4.6 [−2.3, −7.0]	−7.4 [−13.1, −1.7]
P-value (baseline vs. nadir)[a]	≤0.001	≤0.001	0.015
2-minute SpO_2 (%)	97.4 ± 1.7	97.5 ± 1.7	97.3 ± 1.8
Mean difference from baseline SpO_2 (%) [95% CI]	−0.5 [−1.2, 0.1]	−1.0 [−0.2, −1.8]	0.0 [−1.0, 1.0]
P-value (baseline vs. 2-minute)[a]	0.11	0.024	1.0

[a] *P*-value ≤ 0.05 is significant

CF cystic fibrosis, *CI* confidence interval, *HV* healthy volunteer, *SpO_2* blood oxygenation

Table 4

Summary of mean ± standard deviation heart rate changes during HP ^{129}Xe imaging for children receiving full dosing of xenon gas

	All children (*n*=23)	Controls, up to 1/6 TLC dose (*n*=12)	CF subjects, up to 1/6 TLC dose (*n*=11)
Calibration dose			
Baseline HR (bpm)	78.7 ± 14.3	79.2 ± 15.1	78.3 ± 14.0
Nadir HR[a] (bpm)	80.3 ± 13.1	79.9 ± 16.3	80.6 ± 9.3
Mean difference from baseline (bpm) [95% CI]	1.5 [−2.7, 5.7]	0.8 [−5.2, 6.7]	2.4 [−4.6, 9.4]
P-value[b] (baseline vs. nadir)	0.46	0.79	0.47
2-minute HR (bpm)	78.4 ± 13.6	78.3 ± 13.8	78.6 ± 14.1
Mean difference from baseline (bpm) [95% CI]	−0.3 [−3.3, 2.7]	−1.0 [−3.8, 1.9]	0.4 [−5.8, 6.6]
P-value[b] (baseline vs. 2-minute)	0.84	0.50	0.90
Imaging dose			
Baseline HR (bpm)	76.9 ± 13.1	77.8 ± 15.0	76.0 ± 11.3
Nadir HR[a] (bpm)	83.5 ± 16.6	85.3 ± 17.3	80.4 ± 16.3
Mean difference from baseline (bpm) [95% CI]	6.6 [1.1, 12.1]	7.5 [−0.7, 15.7]	5.5 [−3.0, 14.1]
P-value[b] (baseline vs. nadir)	0.021	0.070	0.18
2-minute HR (bpm)	78.0 ± 12.8	79.3 ± 14.4	76.7 ± 11.3
Mean difference from baseline (bpm) [95% CI]	1.1 [−1.3, 3.5]	1.5 [−2.0, 5.0]	0.7 [−3.1, 4.4]
P-value[b] (baseline vs. 2-minute)	0.35	0.37	0.69

bpm beats per minute, *CF* cystic fibrosis, *CI* confidence interval, *HR* heart rate, *TLC* total lung capacity

[a] Nadir HR is the heart rate recorded at the time of the SpO_2 nadir

[b] *P*-value ≤ 0.05 is significant